TWO-POLARISATION FINITE DIFFERENCE MODEL OF BOWED STRINGS WITH NONLINEAR CONTACT AND FRICTION FORCES

Charlotte Desvages, *

Acoustics and Audio Group
The University of Edinburgh
Edinburgh, UK
s1260130@sms.ed.ac.uk

Stefan Bilbao

Acoustics and Audio Group
The University of Edinburgh
Edinburgh, UK
stefan.bilbao@ed.ac.uk

ABSTRACT

Recent bowed string sound synthesis has relied on physical modelling techniques; the achievable realism and flexibility of gestural control are appealing, and the heavier computational cost becomes less significant as technology improves. A bowed string is simulated in two polarisations by discretising the partial differential equations governing its behaviour, using the finite difference method; a globally energy balanced scheme is used, as a guarantee of numerical stability under highly nonlinear conditions. In one polarisation, a nonlinear contact model is used for the normal forces exerted by the dynamic bow hair, left hand fingers, and fingerboard. In the other polarisation, a force-velocity friction curve is used for the resulting tangential forces. The scheme update requires the solution of two nonlinear vector equations.Sound examples and video demonstrations are presented.

1. INTRODUCTION

Physical modelling synthesis for strings debuted in the 1970s, with time stepping methods to discretise the 1D wave equation [1, 2]. However, the very limited computational power at the time ruled out simulation at an audio sample rate in any reasonable amount of time. The next generation of models therefore focussed on algorithmic simplification, through physically plausible assumptions. The non-physical Karplus-Strong string synthesis algorithm [3] was followed by physical digital waveguide models [4]; Karjalainen et al. [5] review the use of these models for string synthesis. Their fast execution and realistic sound output found efficient applications in bowed string modelling, and are still widely used to this day [6, 7, 8, 9, 10]. Another class of physical models relies on the modal solutions of the string equation, and have been successfully adapted for bowed strings [11, 12].

However, the very assumptions that underlie the efficiency of these methods can lead to difficulties when extensions to more realistic settings are desired—the bowed string and its complex interaction with the environment being an excellent example. Time-stepping methods, and more specifically finite difference methods [13], though computationally costly, have regained appeal in musical sound synthesis [14] with the great computing power increase during the last two decades. String simulation in one dimension is particularly suited for these kind of methods [15, 16].

In this work, a linear bowed string is simulated in two polarisations. The model includes full distributed nonlinear contact and friction interactions between the string and the dynamic left hand fingers, dynamic bow, and fingerboard. A stable finite difference scheme for modelling distributed contact/collisions has recently been established [17, 18], that we can use in this stopped string-fingerboard setup [19, 20]. The friction force nonlinearity is modelled with a force/velocity friction curve for the bow [21]; tangential Coulomb friction also keeps the string captured between the fingers and fingerboard during note production. This time domain model allows for full control over the physical parameters of the system, as well as dynamic variations of the playing parameters; it is therefore able to reproduce most bowed string gestures.

In Section 2, the model equations for the bow/string system are presented, with an elaborate description of finger/string interaction in the case of stopped notes, and the string/fingerboard collision interaction. A globally energy balanced finite difference scheme is presented in Section 3. Finally, bowed string simulation results, with the reproduction of several typical gestures, are presented in Section 4. Some sound and video examples from the computed simulations are available online. [1]

2. MODEL DESCRIPTION

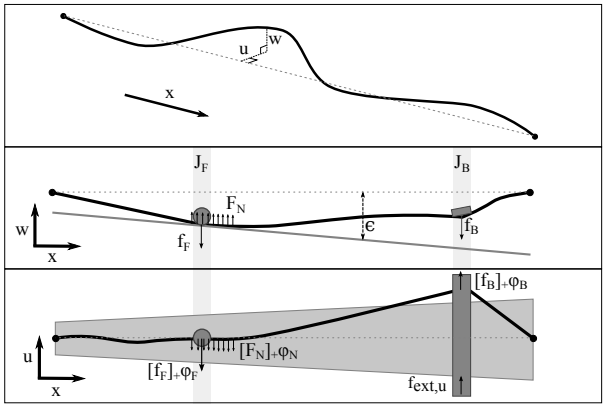

Figure 1: Choice of coordinates for the model. The string is simply supported at both ends. Fingerboard, bow, and left hand finger all interact with the strings in both the vertical and horizontal polarisations. Top: free string. Middle: vertical polarisation. Bottom: horizontal polarisation.

Consider a linear, stiff, and lossy string model in two polarisations. The string displacement in the *vertical* or *normal* polarisation is denoted by $w(x,t)$, while $u(x,t)$ is the string displacement in the

* This work was supported by the Edinburgh College of Art, the Audio Engineering Society, and the European Research Council under grant number StG-2011-279068-NESS.

[1] http://www.ness-music.eu/target-systems/more/bowed-string-instruments

horizontal or *tangential* polarisation. Both are defined for position $x \in \mathcal{D}_S = [0;L]$ and time $t \in \mathbb{R}^+$ (see Figure 1, top).

In this work, consider a single string model, excited by one bow and one finger, and in contact with a fingerboard. The model extends trivially to the case of multiple strings, fingers and bows.

2.1. Vertical polarisation

The partial differential equation governing the time evolution of $w(x,t)$ can be written as:

$$\mathcal{L}w = \mathcal{F}_N - J_F f_F - J_B f_B \tag{1}$$

$\mathcal{L}$ is the partial differential operator defined as [16]:

$$\mathcal{L} = \rho\partial_t^2 - T\partial_x^2 + EI_0\partial_x^4 + \lambda_1\rho\partial_t - \lambda_2\rho\partial_t\partial_x^2 \tag{2}$$

where ρ is the linear mass density of the string, in kg/m; T is the tension of the string, in N; EI_0 is the bending stiffness, where E is Young's modulus in Pa, and $I_0 = \frac{\pi r^4}{4}$ is the area moment of inertia of the circular cross-section of the string, with r the string radius in m; λ_1 (1/s) and λ_2 (m^2/s) are damping coefficients, that empirically account for frequency independent and dependent losses in the string, respectively. $\partial_\cdot^i$ is equivalent to $\frac{\partial^i}{\partial \cdot^i}$.

$\mathcal{L}$ is accompanied by a set of boundary conditions (four of them for the stiff string). We choose standard energy conserving conditions of the simply supported type, assuming an isolated string, with no interaction with the instrument body:

$$w(0,t) = w(L,t) = 0 \qquad \partial_t^2 w(0,t) = \partial_t^2 w(L,t) = 0 \tag{3}$$

The right hand side of Equation 1 contains terms modelling the contact force densities exerted by, respectively, the fingerboard or neck, the left hand finger, and the bow. Their expressions will be elaborated in the following sections.

2.1.1. Fingerboard

$\mathcal{F}_N$ is the contact force density exerted by the neck on the string, along its length (in N/m). Here, a Hunt and Crossley [22] collision model is used, as a smooth approximation to a rigid collision:

$$\mathcal{F}_N(\Delta_N) = \frac{\partial_t \Phi_N}{\partial_t \Delta_N} + \partial_t \Delta_N \Psi_N \tag{4}$$

$\Phi_N(\Delta_N)$ and $\Psi_N(\Delta_N)$ are functions of the *penetration* $\Delta_N(x,t)$, corresponding to the distance by which the edge of the colliding object (here, the fingerboard) would deform from its resting shape:

$$\Phi_N = \frac{K_N}{\alpha_N + 1}[\Delta_N]_+^{\alpha_N+1} \qquad \Psi_N = K_N \beta_N [\Delta_N]_+^{\alpha_N} \tag{5a}$$

$$\Delta_N(x,t) = \varepsilon(x) - w(x,t) \tag{5b}$$

where $K_N > 0$, and $\alpha_N > 1$ are related to the fingerboard stiffness, and $\beta_N > 0$ is a damping coefficient. K_N is chosen very large to approach an ideally rigid collision. $[\cdot]_+$ means $\max(\cdot, 0)$. $\varepsilon(x)$ is the position of the fingerboard with respect to the string at rest (i.e., the action of the instrument; see Figure 1, middle).

2.1.2. Finger and bow

The forces exerted by the finger and the bow onto the string are respectively denoted by $f_F(t)$ and $f_B(t)$. Their action on the string is localised as defined by the continuous distributions $J_F(x,t)$ and $J_B(x,t)$, possibly time-varying (one can use, e.g., a delta Dirac function to model a point wise interaction). $f_F(t)$ and $f_B(t)$ can be written, again, using the Hunt and Crossley model:

$$f_F(\Delta_F) = \frac{\dot{\Phi}_F}{\dot{\Delta}_F} + \dot{\Delta}_F \Psi_F \quad f_B(\Delta_B) = \frac{\dot{\Phi}_B}{\dot{\Delta}_B} + \dot{\Delta}_B \Psi_B \tag{6}$$

where the dot notation is used for total time differentiation ($\frac{d}{dt}$).

$\Phi_F(\Delta_F)$, $\Phi_B(\Delta_B)$, $\Psi_F(\Delta_F)$, and $\Psi_B(\Delta_B)$ are, as for the neck, functions of the penetration $\Delta_F(t)$ and $\Delta_B(t)$:

$$\Phi_F = \frac{K_F}{\alpha_F + 1}[\Delta_F]_+^{\alpha_F+1} \qquad \Psi_F = K_F \beta_F [\Delta_F]_+^{\alpha_F} \tag{7a}$$

$$\Phi_B = \frac{K_B}{\alpha_B + 1}[\Delta_B]_+^{\alpha_B+1} \qquad \Psi_B = K_B \beta_B [\Delta_B]_+^{\alpha_B} \tag{7b}$$

$$\Delta_F(t) = \int_{\mathcal{D}_S} J_F(x,t) w(x,t) dx - w_F(t) \tag{7c}$$

$$\Delta_B(t) = \int_{\mathcal{D}_S} J_B(x,t) w(x,t) dx - w_B(t) \tag{7d}$$

Here, $w_F(t)$ and $w_B(t)$ are respectively the vertical positions of the finger and bow at time t. Their behaviour is governed by:

$$M_F \ddot{w}_F = f_F + f_{\mathrm{extw},F} \tag{8a}$$

$$M_B \ddot{w}_B = f_B + f_{\mathrm{extw},B} \tag{8b}$$

where M_F, M_B are the finger and bow masses, respectively (in kg), and $f_{\mathrm{extw},F}(t)$, $f_{\mathrm{extw},B}(t)$ are the resulting external forces applied vertically on the finger and bow, respectively (in N).

2.2. Horizontal polarisation

The tangential displacement of the string $u(x,t)$ obeys:

$$\mathcal{L}u = -[\mathcal{F}_N]_+ \varphi_N - J_F [f_F]_+ \varphi_F - J_B [f_B]_+ \varphi_B \tag{9}$$

where $\mathcal{L}$, $\mathcal{F}_N$, J_F, f_F, J_B, f_B are defined in Section 2.1. Figure 1, bottom, depicts the tangential forces at play. As for the vertical polarisation, the simply supported boundary conditions are:

$$u(0,t) = u(L,t) = 0 \qquad \partial_t^2 u(0,t) = \partial_t^2 u(L,t) = 0 \tag{10}$$

φ_N, φ_F and φ_B are friction coefficients, depending on the relative velocity of the string with respect to each object. The resulting friction characteristic, or friction curve, differs for the three objects. Indeed, while φ_B has received a lot of experimental interest for rosin-coated bow hair [23], the friction characteristics of the fingerboard and the human fingers is not well known.

In all three cases, however, the friction coefficient is modulated by the normal force applied on the string (derived from the contact model in Section 2.1). As a result, the interactions in the vertical polarisation feed into the horizontal polarisation. It is important to note that this is the coupling point between the two directions of vibration; although definitely worth investigating, intrinsic and/or boundary coupling between the two polarisations is not included in the present model. We consider that the neck, finger and bow are not adhesive, therefore friction exists only for positive normal forces.

2.2.1. Fingerboard

The fingerboard friction coefficient is distributed along the length of the string. To the authors' knowledge, there is no experimental data allowing us to calibrate this friction curve. As the fingerboard (and, as detailed later in Section 2.2.2, the fingers) serves to capture the string to play notes, we can reasonably assume a Coulomb-like characteristic (illustrated in Figure 2a), where the static friction case occurs in most playing situations:

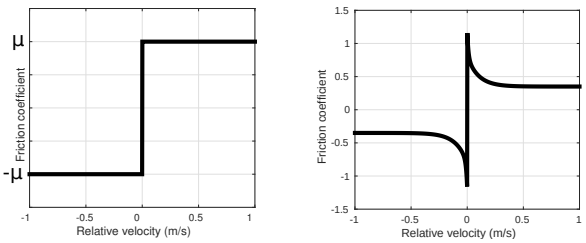

(a) Coulomb friction characteristic. (b) Friction characteristic for the bow, from Smith et al. [23].

Figure 2: Friction curves for (a) neck and finger, and ((b)) bow.

$$\begin{cases} |\varphi_N(v_{\mathrm{rel},N})| \leqslant \mu_N & \text{if } v_{\mathrm{rel},N} = 0 \text{ (static)} \\ \varphi_N(v_{\mathrm{rel},N}) = \mu_N \mathrm{sign}(v_{\mathrm{rel},N}) & \text{if } v_{\mathrm{rel},N} \neq 0 \text{ (kinetic)} \end{cases} \tag{11a}$$

$$v_{\mathrm{rel},N}(x,t) = \partial_t u \tag{11b}$$

2.2.2. *Fingers*

The fingers have the joint function, along with the fingerboard, of capturing the string to reduce its speaking length, to a crude approximation. Assuming a friction characteristic similar to that of the fingerboard leads to:

$$\begin{cases} |\varphi_F(v_{\mathrm{rel},F})| \leqslant \mu_F & \text{if } v_{\mathrm{rel},F} = 0 \text{ (static)} \\ \varphi_F(v_{\mathrm{rel},F}) = \mu_F \mathrm{sign}(v_{\mathrm{rel},F}) & \text{if } v_{\mathrm{rel},F} \neq 0 \text{ (kinetic)} \end{cases} \tag{12a}$$

$$v_{\mathrm{rel},F}(t) = \frac{d}{dt}\left(\int_{\mathcal{D}_\mathcal{S}} J_F(x,t)u(x,t) - u_F(t)\right)dx \tag{12b}$$

$u_F(t)$ is the horizontal position of the fingertip, with respect to the resting string axis. We can hypothesise that the fingertip oscillates about the top finger joint, while simultaneously damping the horizontal vibrations of the string. We can therefore write the temporal evolution of $u_F(t)$ as:

$$M_F \ddot{u}_F = -K_F u_F - \lambda_F \dot{u}_F + [f_F]_+ \varphi_F \tag{13}$$

where λ_F is a damping coefficient. We opt for a linear damped oscillator model for the finger in the horizontal polarisation. Indeed, the choice of a more elaborate contact model such as the one used in the vertical polarisation seems unjustified;while impacts are dominant in the vertical polarisation, e.g. when hammering the string for changing notes, it is clear that collisions only have an auxiliary effect in the tangential polarisation.

2.2.3. *Bow*

The choice of a friction coefficient depending on relative velocity, $\varphi_B(v_{\mathrm{rel},B})$, is somewhat of a trade-off between computational simplification and physical realism. More elaborate models for the bowed string friction interaction, involving viscothermal effects in the rosin layer coating the bow hair, can be used [9, 10]; however, they require significantly more advanced implementations. The friction curve employed here for the bow is indeed deduced from experimental measurements in the steady sliding case (e.g., at constant velocity) [23]; it is illustrated in Figure 2b.

$$\varphi_B = \mathrm{sign}(v_{\mathrm{rel},B})\left(0.4e^{\frac{-|v_{\mathrm{rel},B}|}{0.01}} + 0.45e^{\frac{-|v_{\mathrm{rel},B}|}{0.1}} + 0.35\right) \tag{14a}$$

$$v_{\mathrm{rel},B}(t) = \frac{d}{dt}\left(\int_{\mathcal{D}_\mathcal{S}} J_B(x,t)u(x,t) - u_B(t)\right)dx \tag{14b}$$

where $u_B(t)$ is the bow transverse displacement. The bow, as opposed to the finger, does not oscillate around an equilibrium position, but is pushed across the string:

$$M_B \ddot{u}_B = -\lambda_B \ddot{u}_B + [f_B]_+ \varphi_B + f_{\mathrm{ext}u,B} \tag{15}$$

where λ_B is a coefficient quantifying the linear energy absorption by the bow hair in the horizontal direction, and $f_{\mathrm{ext}u,B}(t)$ is the force with which the player pushes the bow tangentially, in order to establish the desired bow velocity. Note the slight difference with the usual control parameter in most bowed string studies; instead of directly imposing a bow velocity $v_B(t)$, we use the force applied by the player on the bow, resulting in a bow velocity $\ddot{u}_B$.

2.3. Energy analysis

We can derive a power balance equation for both polarisations. The transfer of this equation to discrete time provides a tool to help ensure numerical stability.

Multiplying Equation 1 by $\partial_t w$ and integrating over the length of the string yields the following power balance (for energy-conserving boundary conditions, such as those given in 3):

$$\dot{H}_w = P_w - Q_w \tag{16}$$

The variation of the total kinetic and potential energy $H_w(t) = H_{w,s}(t) + H_{w,N}(t) + H_{w,F}(t) + H_{w,B}(t)$ is equal to the total power $P_w(t)$ withdrawn from or supplied to the system through external excitation, minus the power $Q_w(t) \geqslant 0$ escaping the system through damping. The system is therefore globally energy conserving. The energy is defined as:

$$H_w = H_{w,s} + H_{w,N} + H_{w,F} + H_{w,B} \tag{17a}$$

$$H_{w,s} = \int_{\mathcal{D}_\mathcal{S}} \left[\frac{\rho}{2}(\partial_t w)^2 + \frac{T}{2}(\partial_x w)^2 + \frac{EI_0}{2}\left(\partial_x^2 w\right)^2\right]dx \tag{17b}$$

$$H_{w,N} = \int_{\mathcal{D}_\mathcal{S}} \Phi_N dx \qquad H_{w,F,B} = \Phi_{F,B} + \frac{M_{F,B}}{2}\dot{w}_{F,B}^2 \tag{17c}$$

The power supplied through external excitation is:

$$P_w = \dot{w}_F f_{\mathrm{ext}w,F} + \dot{w}_B f_{\mathrm{ext}w,B} + \int_{\mathcal{D}_\mathcal{S}} (f_F w \partial_t J_F + f_B w \partial_t J_B)dx \tag{18}$$

The power lost through damping within the string and through collision with the neck, finger and bow is given by:

$$Q_w = Q_{w,s} + Q_\Psi \tag{19a}$$

$$Q_{w,s} = \rho \int_{\mathcal{D}_\mathcal{S}} \left[\lambda_1 (\partial_t w)^2 + \lambda_2 (\partial_t \partial_x w)^2\right]dx \tag{19b}$$

$$Q_\Psi = \int_{\mathcal{D}_\mathcal{S}} (\partial_t \Delta_N)^2 \Psi_N dx + \dot{\Delta}_F^2 \Psi_F + \dot{\Delta}_B^2 \Psi_B \tag{19c}$$

In the absence of excitation, the energy H_w strictly decreases.

For the horizontal polarisation, multiplying Equation 10 by $\partial_t u$ and integrating over $\mathcal{D}_\mathcal{S}$ yields the power balance:

$$\dot{H}_u = P_u - Q_u \tag{20}$$

Again, the variation of $H_u(t) = H_{u,s}(t) + H_{u,F}(t) + H_{u,B}(t)$ is equal to the total power $P_u(t)$ supplied to or withdrawn from the system in the horizontal polarisation through external excitation, minus power losses $Q_u(t) \geqslant 0$ from damping. The energy is defined as:

$$H_u = H_{u,s} + H_{u,F} + H_{u,B} \tag{21a}$$

$$H_{u,s} = \int_{\mathcal{D}_\mathcal{S}} \left[\frac{\rho}{2} (\partial_t u)^2 + \frac{T}{2} (\partial_x u)^2 + \frac{EI_0}{2} \left(\partial_x^2 u\right)^2 \right] dx \tag{21b}$$

$$H_{u,F} = \frac{M_F}{2} \dot{u}_F^2 + \frac{K_F}{2} u_F^2 \qquad H_{u,B} = \frac{M_B}{2} \dot{u}_B^2 \tag{21c}$$

The power supplied or withdrawn by external excitation is:

$$P_u = [f_F]_+ \varphi_F \int_{\mathcal{D}_\mathcal{S}} u \partial_t J_F dx + [f_B]_+ \varphi_B \int_{\mathcal{D}_\mathcal{S}} u \partial_t J_B dx + \dot{u}_B f_{\mathrm{ext}u,B} \tag{22}$$

The power lost through string damping and friction is:

$$Q_u = Q_{u,s} + Q_\varphi + Q_{u,F} + Q_{u,B} \tag{23a}$$

$$Q_{u,s} = \rho \int_{\mathcal{D}_\mathcal{S}} \left[\lambda_1 (\partial_t u)^2 + \lambda_2 (\partial_t \partial_x u)^2 \right] dx \tag{23b}$$

$$Q_\varphi = \int_{\mathcal{D}_\mathcal{S}} v_{\mathrm{rel},N} [\mathcal{F}_N]_+ \varphi_N dx + v_{\mathrm{rel},F} [f_F]_+ \varphi_F + v_{\mathrm{rel},B} [f_B]_+ \varphi_B \tag{23c}$$

$$Q_{u,F,B} = \lambda_{F,B} \dot{u}_{F,B}^2 \tag{23d}$$

Note that $Q_u \geqslant 0$ if $v_{\mathrm{rel}} \varphi(v_{\mathrm{rel}}) \geqslant 0$, which is true for the friction characteristics of the three objects.

The total power of the full system is therefore balanced by:

$$\dot{H} = P - Q \tag{24a}$$

$$H = H_u + H_w \qquad P = P_u + P_w \qquad Q = Q_u + Q_w \tag{24b}$$

3. NUMERICAL SCHEME

We can now discretise the equations of motion by approximating the partial derivation operators with their finite difference [13] counterparts. This method allows a full system simulation, and therefore great flexibility of control for the input parameters and gesture reproduction, at the cost of increased computational requirements. This method has seen a myriad of applications in physical modelling sound synthesis, and more generally musical acoustics simulations [1, 14]. In this section, we define the numerical scheme, detail the discrete energy balance, and describe the scheme update.

3.1. Grid functions and finite difference (FD) operators

All the varying quantities defined in Section 2 are now discretised into *grid functions*, defined at positions $x = lh, l \in \mathfrak{d}_\mathcal{S} = [0,...,N]$, and times $t = nk, n \in \mathbb{N}$. h is the *grid spacing*, in m; $k = 1/F_s$ is the *time step*, in s, with F_s the sample rate in Hz. For an arbitrary continuous function $g(x,t)$ defined for $x \in \mathcal{D}_\mathcal{S}$ and $t \in \mathbb{R}^+$, g_l^n is a grid function approximating $g(lh,nk)$.

Let us introduce the forward and backward unit time and space shift operators, applied to g_l^n:

$$e_{t-} g_l^n = g_l^{n-1} \qquad e_{t+} g_l^n = g_l^{n+1} \tag{25a}$$

$$e_{x-} g_l^n = g_{l-1}^n \qquad e_{x+} g_l^n = g_{l+1}^n \tag{25b}$$

The partial differentiation with respect to time and space can be approximated with a number of first order FD operators:

$$\delta_{t-} = \frac{1 - e_{t-}}{k} \qquad \delta_{t+} = \frac{e_{t+} - 1}{k} \qquad \delta_{t\cdot} = \frac{e_{t+} - e_{t-}}{2k} \tag{26a}$$

$$\delta_{x-} = \frac{1 - e_{x-}}{h} \qquad \delta_{x+} = \frac{e_{x+} - 1}{h} \tag{26b}$$

Higher order partial derivation operators are approximated with:

$$\partial_t^2 \approx \delta_{tt} = \delta_{t-} \delta_{t+} \qquad \partial_x^2 \approx \delta_{xx} = \delta_{x-} \delta_{x+} \tag{27a}$$

$$\partial_x^4 \approx \delta_{xxxx} = \delta_{xx} \delta_{xx} \tag{27b}$$

Finally, the averaging FD operators approximate identity:

$$\mu_{t-} = \frac{1 + e_{t-}}{2} \qquad \mu_{t+} = \frac{e_{t+} + 1}{2} \qquad \mu_{t\cdot} = \frac{e_{t+} + e_{t-}}{2} \tag{28}$$

Note that $\delta_{t-} \mu_{t+} = \delta_{t+} \mu_{t-} = \delta_{t\cdot}$.

3.2. Vector-matrix notation

A number of grid functions are defined over $\mathfrak{d}_\mathcal{S}$. We can therefore describe the discrete position of the whole string with vectors. The simply supported boundary conditions ensure that the two extreme values are 0 at all times:

$$w_0^n = w_N^n = 0 \qquad u_0^N = u_N^n = 0 \tag{29a}$$

$$\delta_{xx} w_0^n = \delta_{xx} w_N^n = 0 \qquad \delta_{xx} u_0^n = \delta_{xx} u_N^n = 0 \tag{29b}$$

We now only need to store the state of the string in a vector of size $(N-1)$, omitting the two extreme values:

$$\mathbf{w}^n = [w_1^n, ..., w_{N-1}^n]^T \qquad \mathbf{u}^n = [u_1^n, ..., u_{N-1}^n]^T \tag{30}$$

The action of spatial FD operators on the grid functions is then equivalent to a matrix-vector multiplication. For simply supported boundary conditions, the notation of spatial FD operators in matrix form naturally follows as:

$$\mathbf{D}_{x-} = \frac{1}{h} \begin{bmatrix} 1 & & & \\ -1 & 1 & & \\ & \ddots & \ddots & \\ & & -1 & 1 \\ & & & -1 \end{bmatrix} \qquad \begin{aligned} \mathbf{D}_{x+} &= -\mathbf{D}_{x-}^T \\ \mathbf{D}_{xx} &= \mathbf{D}_{x+} \mathbf{D}_{x-} \\ \mathbf{D}_{xxxx} &= \mathbf{D}_{xx} \mathbf{D}_{xx} \end{aligned} \tag{31}$$

of size $N \times (N-1)$, $(N-1) \times N$, $(N-1) \times (N-1)$, and $(N-1) \times (N-1)$, respectively.

3.3. Finite difference scheme

3.3.1. Vertical polarisation

We can now discretise Equation 1 as follows:

$$\mathsf{L} \mathbf{w}^n = \mu_{t\cdot} \mathbf{J}_\mathbf{w}^n \mathbf{f}_\mathbf{w}^n \tag{32}$$

where L is a matrix form discretisation of the partial derivation operator $\mathcal{L}$ defined in Equation 2:

$$\mathsf{L} = \rho \delta_{tt} - T \mathbf{D}_{xx} + EI_0 \mathbf{D}_{xxxx} + \lambda_1 \rho \delta_{t\cdot} - \lambda_2 \rho \delta_{t-} \mathbf{D}_{xx} \tag{33}$$

$\mathbf{J}_\mathbf{w}^n$ is the $(N-1) \times (N+1)$ distribution matrix, and $\mathbf{f}_\mathbf{w}^n$ is a column vector containing all the contact force information:

$$\mathbf{J}_\mathbf{w}^n = \left[\begin{array}{c|c|c} \mathbf{I_{N-1}} & -\mathbf{j}_F^n & -\mathbf{j}_B^n \end{array} \right] \tag{34a}$$

$$\mathbf{f}_\mathbf{w}^n = \left[\begin{array}{c|c|c} (\mathbf{f}_N^n)^T & f_F^n & f_B^n \end{array} \right]^T \tag{34b}$$

where $\mathbf{I_{N-1}}$ is the $(N-1)\times(N-1)$ identity matrix, and $\mathbf{j}_F^n$ and $\mathbf{j}_B^n$ are discrete spreading operators in column vector form, accounting for the continuous distributions described in Section 2.1.2. $\mathbf{f}_N^n$, f_F^n and f_B^n are the discrete counterparts of those defined in Section 2.1. Energy conserving schemes for lumped collisions have been used for similar problems (in particular, the collision of a piano hammer with the string [24]); one in particular, was recently studied [25], that we adapt for the damped, distributed case [17]. We now have:

$$\mathbf{f}_\mathbf{w}^n = \frac{\delta_t.\mathbf{\Phi}^n}{\delta_t.\mathbf{\Delta}^n} + (\delta_t.\mathbf{\Delta}^n)\odot\mathbf{\Psi}^n \tag{35}$$

where the division is pointwise, and $\odot$ is the pointwise product.

$\mathbf{\Phi}^n(\mathbf{\Delta}^n)$, $\mathbf{\Psi}^n(\mathbf{\Delta}^n)$ are function of the vector penetration $\mathbf{\Delta}^n$:

$$\mathbf{\Phi}^n(\mathbf{\Delta}^n) = \frac{\mathbf{K}}{\boldsymbol{\alpha}+1}\odot[\mathbf{\Delta}^n]_+^{\boldsymbol{\alpha}+1} \quad \mathbf{\Psi}^n(\mathbf{\Delta}^n) = \mathbf{K}\odot\boldsymbol{\beta}\odot[\mathbf{\Delta}^n]_+^{\boldsymbol{\alpha}} \tag{36}$$

where the exponentiation operation is also element-wise. $\mathbf{\Delta}^n$, $\mathbf{K}$, $\boldsymbol{\alpha}$, and $\boldsymbol{\beta}$ are now in vector form:

$$\mathbf{K} = \begin{bmatrix} \vdots \\ K_N \\ \vdots \\ \hline K_F \\ \hline K_B \end{bmatrix} \quad \boldsymbol{\alpha} = \begin{bmatrix} \vdots \\ \alpha_N \\ \vdots \\ \hline \alpha_F \\ \hline \alpha_B \end{bmatrix} \quad \boldsymbol{\beta} = \begin{bmatrix} \vdots \\ \beta_N \\ \vdots \\ \hline \beta_F \\ \hline \beta_B \end{bmatrix} \tag{37a}$$

$$\mathbf{\Delta}^n = \begin{bmatrix} \vdots \\ \mathbf{\Delta}_N^n \\ \vdots \\ \hline \Delta_F^n \\ \hline \Delta_B^n \end{bmatrix} \begin{array}{l} \mathbf{\Delta}_N^n = \varepsilon - \mathbf{w}^n \\ \\ \Delta_F^n = h\mathbf{j}_F^{n\,T}\mathbf{w}^n - w_F^n \\ \\ \Delta_B^n = h\mathbf{j}_B^{n\,T}\mathbf{w}^n - w_B^n \end{array} \tag{37b}$$

where $\varepsilon_l = \varepsilon(lh)$, and w_F^n and w_B^n are the respective vertical positions of the finger and bow, governed by:

$$\mathbf{M}_{FB}\delta_{tt}\mathbf{w}_{FB}^n = \mathbf{f}_{\mathbf{w}FB}^n + \mathbf{f}_{\mathbf{ext}w,FB}^n \qquad \mathbf{M}_{FB} = \begin{bmatrix} M_F & 0 \\ 0 & M_B \end{bmatrix} \tag{38a}$$

$$\mathbf{w}_{FB}^n = \begin{bmatrix} w_F^n \\ w_B^n \end{bmatrix} \qquad \mathbf{f}_{\mathbf{w}FB}^n = \begin{bmatrix} f_F^n \\ f_B^n \end{bmatrix} \qquad \mathbf{f}_{\mathbf{ext}w,FB}^n = \begin{bmatrix} f_{\mathrm{ext}w,F}^n \\ f_{\mathrm{ext}w,B}^n \end{bmatrix} \tag{38b}$$

3.3.2. Horizontal polarisation

Equation 9 is now discretised as:

$$\mathsf{L}\mathbf{u}^n = -\mu_t.\mathbf{J}_\mathbf{u}^n\mathbf{f}_\mathbf{u}^n \tag{39a}$$

$$\mathbf{J}_\mathbf{u}^n = \left[\begin{array}{c|c|c} \mathbf{I_{N-1}} & \mathbf{j}_F^n & \mathbf{j}_B^n \end{array}\right] \tag{39b}$$

L is defined in Equation 33. $\mathbf{f}_\mathbf{u}^n$ is a column vector containing the friction force information:

$$\mathbf{f}_\mathbf{u}^n = \begin{bmatrix} \vdots \\ [\mathbf{f}_N^n]_+\odot\varphi_N\left(\mathbf{v}_{\mathrm{rel},N}^n\right) \\ \vdots \\ \hline [f_F^n]_+\varphi_F\left(v_{\mathrm{rel},F}^n\right) \\ \hline [f_B^n]_+\varphi_B\left(v_{\mathrm{rel},B}^n\right) \end{bmatrix} \begin{array}{l} \mathbf{v}_{\mathrm{rel},N}^n = \delta_t.\mathbf{u}^n \\ \\ v_{\mathrm{rel},F}^n = h\delta_t.\left(\mathbf{j}_F^{n\,T}\mathbf{u}^n\right) - \delta_t.u_F^n \\ \\ v_{\mathrm{rel},B}^n = h\delta_t.\left(\mathbf{j}_B^{n\,T}\mathbf{u}^n\right) - \delta_t.u_B^n \end{array} \tag{40}$$

where φ_N, φ_F and φ_B are defined in section 2.2. We can define a vector relative velocity:

$$\mathbf{v}_\mathrm{rel}^n = \left[\left(\mathbf{v}_{\mathrm{rel},N}^n\right)^T | v_{\mathrm{rel},F}^n | v_{\mathrm{rel},B}^n\right]^T \tag{41}$$

Finally, a matrix equation describes the evolution of the horizontal displacements u_F^n and u_B^n of the finger and bow, respectively:

$$\mathbf{M}_{FB}\delta_{tt}\mathbf{u}_{FB}^n = \mathbf{K}_{FB}\mu_t.\mathbf{u}_{FB}^n - \boldsymbol{\lambda}_{FB}\delta_t.\mathbf{u}_{FB}^n + \mathbf{f}_{\mathbf{u}FB}^n + \mathbf{f}_{\mathbf{ext}u,FB}^n \tag{42a}$$

$$\mathbf{K}_{FB} = \begin{bmatrix} K_F & 0 \\ 0 & 0 \end{bmatrix} \quad \boldsymbol{\lambda}_{FB} = \begin{bmatrix} \lambda_F & 0 \\ 0 & \lambda_B \end{bmatrix} \quad \mathbf{u}_{FB}^n = \begin{bmatrix} u_F^n \\ u_B^n \end{bmatrix} \tag{42b}$$

$$\mathbf{f}_{\mathbf{u}FB}^n = \begin{bmatrix} [f_F^n]_+\varphi_F\left(v_{\mathrm{rel},F}^n\right) \\ [f_B^n]_+\varphi_B\left(v_{\mathrm{rel},B}^n\right) \end{bmatrix} \quad \mathbf{f}_{\mathbf{ext}u,FB}^n = \begin{bmatrix} 0 \\ f_{\mathrm{ext}u,B}^n \end{bmatrix} \tag{42c}$$

3.4. Energy analysis

We can transfer the results of Section 2.3 to discrete time, and monitor the energy exchanges going on in the system at all times during the simulation. We derive an energy balance equation between the energy of the closed system (H^n) and the power brought in and out, by external excitation (P^n) and damping Q^n. Conservation of this *total* energy helps ensuring a stable algorithm.

3.4.1. Vertical polarisation

For the vertical polarisation, multiplying Equation 32 by $h(\delta_t.\mathbf{w}^n)^T$ and Equation 38a by $(\delta_t.\mathbf{w}_{FB}^n)^T$ gives the power balance:

$$\delta_{t-}\mathrm{H}_w^n = \mathrm{P}_w^n - \mathrm{Q}_w^n \tag{43}$$

The numerical energy H_w^n is defined as:

$$\mathrm{H}_w^n = \mathrm{H}_{w,s}^n + \mathrm{H}_\Phi^n \tag{44a}$$

$$\mathrm{H}_{w,s}^n = \frac{\rho h}{2}|\delta_{t+}\mathbf{w}^n|^2 + \frac{Th}{2}(\mathbf{D}_{x-}\mathbf{w}^n)^T\mathbf{D}_{x-}\mathbf{w}^{n+1} + \frac{EI_0h}{2}(\mathbf{D}_{xx}\mathbf{w}^n)^T\mathbf{D}_{xx}\mathbf{w}^{n+1} - \frac{\lambda_2\rho kh}{4}|\delta_{t+}\mathbf{D}_{x-}\mathbf{w}^n|^2 \tag{44b}$$

$$\mathrm{H}_\Phi^n = \mathbf{h}^T\mu_{t+}\mathbf{\Phi}^n + \frac{1}{2}(\mathbf{M}_{FB}\delta_{t+}\mathbf{w}_{FB}^n)^T\delta_{t+}\mathbf{w}_{FB}^n \tag{44c}$$

where $\mathbf{h} = [...h...|1|1]^T$.

The power P_w^n supplied or withdrawn through excitation is:

$$\mathrm{P}_w^n = (\delta_t.\mathbf{w}_{FB}^n)^T\mathbf{f}_{\mathrm{ext}w,FB}^n - h\Big(\left(\mu_t.\mathbf{w}^n\right)^T(\delta_t.\mathbf{J}^n)\Big)\mathbf{f}_\mathbf{w}^n \tag{45}$$

The power $\mathrm{Q}_w^n \geqslant 0$ dissipated through damping is:

$$\mathrm{Q}_w^n = \mathrm{Q}_{w,s}^n + \mathrm{Q}_\Psi^n \tag{46a}$$

$$\mathrm{Q}_{w,s}^n = \lambda_1\rho h|\delta_t.\mathbf{w}^n|^2 + \lambda_2\rho h|\delta_t.\mathbf{D}_{x-}\mathbf{w}^n|^2 \tag{46b}$$

$$\mathrm{Q}_\Psi^n = (\mathbf{h}\odot\delta_t.\mathbf{\Delta}^n)^T((\delta_t.\mathbf{\Delta}^n)\odot\mathbf{\Psi}^n) \tag{46c}$$

In the absence of external excitation, the numerical energy H_w^n is strictly decreasing. The stability of this scheme then boils down to H_w^n being non-negative at all times. As $\mathrm{H}_\Phi^n \geqslant 0$ by construction, this is then equivalent to $\mathrm{H}_{w,s}^n \geqslant 0$, which is verified under the condition linking the time step k and grid spacing h [14]:

$$h \geqslant \sqrt{\frac{1}{2}\left(\frac{Tk^2}{\rho} + 2\lambda_2 k + \sqrt{\left(\frac{Tk^2}{\rho} + 2\lambda_2 k\right)^2 + 16k^2\frac{EI_0}{\rho}}\right)} \tag{47}$$

3.4.2. Horizontal polarisation

On the other hand, the product of Equation 36 by $h(\delta_{t\cdot}\mathbf{u}^n)^T$, and that of Equation 42a by $(\delta_{t\cdot}\mathbf{u}^n_{FB})^T$, yields a numerical power balance for the horizontal polarisation:

$$\delta_{t-}\mathrm{H}^n_u = \mathrm{P}^n_u - \mathrm{Q}^n_u \tag{48}$$

where the numerical energy H^n_u is defined as:

$$\mathrm{H}^n_u = \mathrm{H}^n_{u,s} + \mathrm{H}^n_{u,FB} \tag{49a}$$

$$\mathrm{H}^n_{u,s} = \frac{\rho h}{2}|\delta_{t+}\mathbf{u}^n|^2 + \frac{Th}{2}(\mathbf{D}_{x-}\mathbf{u}^n)^T\mathbf{D}_{x-}\mathbf{u}^{n+1} + \frac{EI_0 h}{2}(\mathbf{D}_{xx}\mathbf{u}^n)^T\mathbf{D}_{xx}\mathbf{u}^{n+1} - \frac{\lambda_2\rho k h}{4}|\delta_{t+}\mathbf{D}_{x-}\mathbf{u}^n|^2 \tag{49b}$$

$$\mathrm{H}^n_{u,FB} = \frac{1}{2}(\mathbf{M}_{FB}\delta_{t+}\mathbf{u}^n_{FB})^T\delta_{t+}\mathbf{u}^n_{FB} + \frac{1}{2}\mu_{t+}\Big((\mathbf{K}_{FB}\mathbf{u}^n_{FB})^T\mathbf{u}^n_{FB}\Big) \tag{49c}$$

The power P^n_u brought in or out by the excitation is:

$$\mathrm{P}^n_u = h\Big((\mu_{t\cdot}\mathbf{u}^n)^T(\delta_{t\cdot}\mathbf{J}^n)\Big)\mathbf{f}^n_{\mathbf{u}} + (\delta_{t\cdot}\mathbf{u}^n_{FB})^T\mathbf{f}^n_{\mathbf{ext}u,FB} \tag{50}$$

The power $\mathrm{Q}^t_u \geqslant 0$ dissipated by friction and damping is:

$$\mathrm{Q}^n_u = \mathrm{Q}^n_{u,s} + \mathrm{Q}^n_{\varphi} + \mathrm{Q}^n_{u,FB} \tag{51a}$$

$$\mathrm{Q}^n_{u,s} = \lambda_1\rho h|\delta_{t\cdot}\mathbf{u}^n|^2 + \lambda_2\rho h|\delta_{t\cdot}\mathbf{D}_{x-}\mathbf{u}^n|^2 \tag{51b}$$

$$\mathrm{Q}^n_{\varphi} = (\mathbf{h}\odot\mathbf{v}^n_{\mathrm{rel}})^T\mathbf{f}^n_{\mathbf{u}} \tag{51c}$$

$$\mathrm{Q}^n_{u,FB} = (\lambda_{FB}\delta_{t\cdot}\mathbf{u}_{FB})^T\delta_{t\cdot}\mathbf{u}_{FB} \tag{51d}$$

The stability condition 47 straightforwardly holds for this scheme; indeed, choosing to use the 2-point averaging operator in Equation 42a does not introduce any stricter bound on h, as the energy $\mathrm{H}^n_{u,FB}$ of the finger and bow is always strictly positive.

3.4.3. Total energy

The total numerical energy H^n of the system is balanced by:

$$\delta_{t-}\mathrm{H}^n = \mathrm{P}^n - \mathrm{Q}^n \tag{52a}$$

$$\mathrm{H}^n = \mathrm{H}^n_u + \mathrm{H}^n_w \qquad \mathrm{P}^n = \mathrm{P}^n_u + \mathrm{P}^n_w \qquad \mathrm{Q}^n = \mathrm{Q}^n_u + \mathrm{Q}^n_w \tag{52b}$$

We can therefore monitor the quantity E^n, that should remain constant (to machine accuracy) throughout the simulation:

$$\mathrm{E}^n = \mathrm{H}^n - k\sum_{i=0}^{n}\Big(\mathrm{P}^i - \mathrm{Q}^i\Big) = \mathrm{H}^0 \tag{53}$$

3.5. Scheme update

3.5.1. Vertical polarisation

Expanding the operators in Equations 32 and 38a, and combining 35 and 36, leads to a two-step recursion algorithm in vector-matrix form, to be updated at each time step n:

$$\mathbf{w}^{n+1} = \mathbf{B}\mathbf{w}^n + \mathbf{C}\mathbf{w}^{n-1} + A\mu_{t\cdot}\mathbf{J}^n_{\mathbf{w}}\mathbf{f}^n_{\mathbf{w}} \tag{54a}$$

$$\mathbf{w}^{n+1}_{FB} = 2\mathbf{w}^n_{FB} - \mathbf{w}^{n-1}_{FB} + k^2\mathbf{M}^{-1}_{FB}\big(\mathbf{f}^n_{\mathbf{w}FB} + \mathbf{f}^n_{\mathbf{ext}w,FB}\big) \tag{54b}$$

$$A = \frac{2k^2}{\rho(2+\lambda_1 k)} \tag{54c}$$

$$\mathbf{B} = \frac{2}{2+\lambda_1 k}\left(2 + \left(\frac{Tk^2}{\rho} + \lambda_2 k\right)\mathbf{D}_{xx} - \frac{EI_0 k^2}{\rho}\mathbf{D}_{xxxx}\right) \tag{54d}$$

$$\mathbf{C} = \frac{2}{2+\lambda_1 k}\left(\frac{\lambda_1 k}{2} - 1 - \lambda_2 k\mathbf{D}_{xx}\right) \tag{54e}$$

However, the nonlinearity of the contact model doesn't allow for a simple explicit update. Combining Equations 54a and 54b, and rewriting in terms of $\boldsymbol{\Delta}^n$, leads to a nonlinear equation in matrix form, in terms of the unknown vector $\mathbf{r}^n = \boldsymbol{\Delta}^{n+1} - \boldsymbol{\Delta}^{n-1}$:

$$\boldsymbol{\Lambda}^n_1\mathrm{r}^n + \boldsymbol{\Lambda}_2{}^n\mathbf{f}^n_{\Phi} + \mathbf{b}^n_{\mathbf{w}} = 0 \tag{55}$$

where the matrices $\boldsymbol{\Lambda}^n_1$, $\boldsymbol{\Lambda}^n_2$, and the vectors $\mathbf{f}^n_{\Phi}$, $\mathbf{b}^n$ are given by:

$$\boldsymbol{\Lambda}^n_2 = A\mathrm{diag}(\overline{\mathbf{h}})\big(\mathbf{J}^{n+1}_{\mathbf{w}}\big)^T\mu_{t\cdot}\mathbf{J}^n_{\mathbf{w}} + k^2\mathbf{M}_{\mathrm{inv}} \tag{56a}$$

$$\boldsymbol{\Lambda}^n_1 = \mathbf{I}_{\mathbf{N+1}} + \frac{1}{2k}\boldsymbol{\Lambda}^n_2\mathrm{diag}(\boldsymbol{\Psi}^n) \tag{56b}$$

$$\mathbf{f}^n_{\Phi} = \frac{\delta_{t\cdot}\boldsymbol{\Phi}^n}{\delta_{t\cdot}\boldsymbol{\Delta}^n} = \frac{\boldsymbol{\Phi}(\mathbf{r}^n + \boldsymbol{\Delta}^{n-1}) - \boldsymbol{\Phi}(\boldsymbol{\Delta}^{n-1})}{\mathbf{r}^n} \tag{56c}$$

$$\mathbf{b}^n_{\mathbf{w}} = \Big[\mathbf{0_{N-1}}|2\big(\mathbf{w}^n_{FB} - \mathbf{w}^{n-1}_{FB}\big)^T + k^2\big(\mathbf{M}^{-1}_{FB}\mathbf{f}^n_{\mathbf{ext},\mathrm{FB}}\big)^T\Big]^T + \mathrm{diag}(\overline{\mathbf{h}})\Big(\big(\mathbf{J}^{n+1}_{\mathbf{w}}\big)^T\big(\mathbf{B}\mathbf{w}^n + \mathbf{C}\mathbf{w}^{n-1}\big) - \big(\mathbf{J}^{n-1}_{\mathbf{w}}\big)^T\mathbf{w}^{n-1}\Big) \tag{56d}$$

where $\mathbf{M}_{\mathrm{inv}}$ is a $(N+1)\times(N+1)$ matrix with $\mathbf{M}^{-1}_{FB}$ at its bottom-right corner, and all zeros elsewhere; $\mathbf{0_{N-1}}$ is an all-zero row vector of length $(N-1)$; and $\overline{\mathbf{h}} = [...1...|h|h]^T$.

Equation 55 is resolved with an iterative nonlinear system solver.

3.5.2. Horizontal polarisation

Similarly to the vertical polarisation, a two-step recursion is derived from Schemes 39a and 42a:

$$\mathbf{u}^{n+1} = \mathbf{B}\mathbf{u}^n + \mathbf{C}\mathbf{u}^{n-1} - A\mu_{t\cdot}\mathbf{J}^n_{\mathbf{u}}\mathbf{f}^n_{\mathbf{u}} \tag{57a}$$

$$\mathbf{u}^{n+1}_{FB} = \mathbf{B}_{FB}\mathbf{u}^n_{FB} + \mathbf{C}^{n-1}_{FB} + k^2\mathbf{M}^{-1}_{FB}\mathbf{A}_{FB}\big(\mathbf{f}^n_{\mathbf{u}FB} + \mathbf{f}^n_{\mathbf{ext}u,FB}\big) \tag{57b}$$

$$\mathbf{A}_{FB} = 2\big(2\mathbf{M}_{FB} + k^2\mathbf{K}_{FB} + k\boldsymbol{\lambda}_{FB}\big)^{-1}\mathbf{M}_{FB} \tag{57c}$$

$$\mathbf{B}_{FB} = 2\mathbf{A}_{FB} \tag{57d}$$

$$\mathbf{C}_{FB} = \frac{1}{2}\mathbf{A}_{FB}\big(-2\mathbf{M}_{FB} - k^2\mathbf{K}_{FB} + k\boldsymbol{\lambda}_{FB}\big)\mathbf{M}^{-1}_{FB} \tag{57e}$$

A, $\mathbf{B}$, and $\mathbf{C}$ are defined in 54. We can write Equations 57a and 57b in terms of $\mathbf{v}^n_{\mathrm{rel}}$:

$$\mathbf{v}^n_{\mathrm{rel}} + \boldsymbol{\Lambda}^n_3\mathbf{f}^n_{\mathbf{u}} + \mathbf{b}^n_{\mathbf{u}} = 0 \tag{58}$$

where the matrix $\boldsymbol{\Lambda}^n_3$, and the vector $\mathbf{b}^n_{\mathbf{u}}$ are defined as:

$$\mathbf{\Lambda}_3^n = \frac{1}{2k}\left(A\mathrm{diag}\left(\overline{\mathbf{h}}\right)\left(\mathbf{J}_\mathbf{u}^{n+1}\right)^T \mu_t.\mathbf{J}_\mathbf{u}^n + \mathbf{A}_{\mathrm{obj}}\right) \tag{59a}$$

$$\mathbf{b}_\mathbf{u}^n = \frac{1}{2k}\mathrm{diag}\left(\overline{\mathbf{h}}\right)\left(\left(\mathbf{J}_\mathbf{u}^{n-1}\right)^T \mathbf{u}^{n-1} - \left(\mathbf{J}_\mathbf{u}^{n+1}\right)^T\left(\mathbf{B}\mathbf{u}^n + \mathbf{C}\mathbf{u}^{n-1}\right)\right) + \left[\mathbf{0_{N-1}}|(\mathbf{b}_{\mathbf{u}FB}^n)^T\right]^T \tag{59b}$$

$$\mathbf{b}_{\mathbf{u}FB}^n = \frac{1}{2k}\left(\mathbf{B}_{FB}\mathbf{u}_{FB}^n + (\mathbf{C}_{FB} - \mathbf{I_2})\mathbf{u}_{FB}^{n-1} + \mathbf{A}_{FB}\mathbf{f}_{\mathbf{ext}u,FB}^n\right) \tag{59c}$$

where $\mathbf{A}_{\mathrm{obj}}$ is a $(N+1)\times(N+1)$ matrix with $\mathbf{A}_{FB}$ at its bottom-right corner and zeros elsewhere; $\mathbf{I_2}$ is the 2×2 identity matrix.

4. SIMULATION RESULTS

4.1. Control parameters

Simulations are run at audio sample rate (F_s = 44.1 kHz). The user controls the physical parameters of the string and all three objects. A table of measured string parameters on violins, violas and cellos (from Percival [26]) is readily available as a preset. The gestural control is achieved with breakpoint functions for the bow position, force applied normally and tangentially, and the finger position and normal force. The output waveform is read as the displacement of the last mobile point of the string before the bridge termination.

A video demonstrating a typical gesture, generated from simulated data from this model, is available on the companion website [1].

4.2. Bowed string motion

As the bow is driven by an external force, and not an imposed velocity, the amplitude and shape of the force signal to send into the bow is at first less intuitive to gauge. However, while a full parameter exploration study is definitely worth considering (with regards to playability and transient quality; see e.g. [27]), minimal trial and error allowed us to successfully reproduce the standard, periodic Helmholtz motion of the bowed string, as well as other typical oscillation states under realistic bowing conditions. Schelleng [28] described theoretical bow force limits, for a given bow position and velocity, beyond which the player presses the bow either too strongly for the returning Helmholtz corner to detach it from the string (*raucous motion*), or too lightly for the string to stick to it for a whole nominal period (*multiple slipping*). Figure 3 shows the typical sawtooth waveform associated with the Helmholtz motion, the split sawtooth associated with multiple slipping, and the rough, aperiodic waveform resulting from raucous motion of the string.

4.3. Gesture reproduction

The inclusion of the left hand finger and neck, as well as the dynamics of the bow, allow to simulate a broad range of typical bowed string gestures. The bow can move along and bounce against the string; the fingers sliding along the fingerboard or oscillating around a central position create glissando and vibrato sounds. "Plucking" the string with a half raised cosine function in both polarisations leads to pizzicato sounds, and even slap double bass, if the string is plucked hard enough to bounce and rub against the fingerboard.

4.4. Energy balance

To demonstrate the balanced numerical energy of the system, we monitor the variations of the quantity E^n defined in Equation 53 along a bowed string simulation, where the bow and finger positions, forces, and the bow tangential force are all time-varying. We

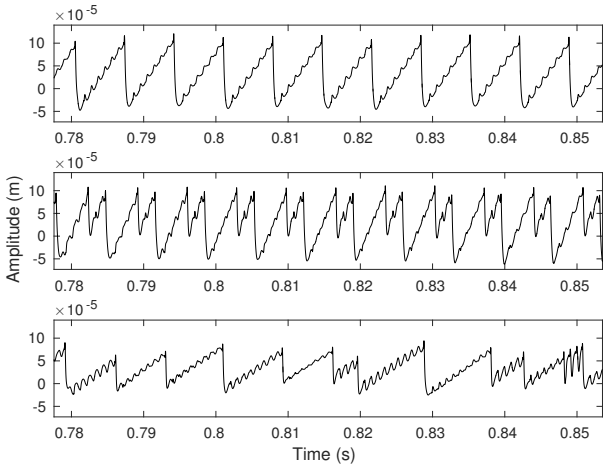

Figure 3: Different simulated waveforms on a cello D string, with fixed bow position $x_B = 0.851L$ m, bow force $f_{\mathrm{ext}w,B} = -2$ N, and bow tangential force $f_{\mathrm{ext}u,B} = 4.4$ N (Helmholtz motion, top), $f_{\mathrm{ext}u,B} = 6.8$ N (multiple slipping, middle), and $f_{\mathrm{ext}u,B} = 2.5$ N (raucous motion, bottom).

normalise E^n with respect to the mean energy $\bar{\mathrm{H}}^n$, averaged over the duration of the simulation. As seen in Figure 4 (bottom), E^n is invariant until the 10th significant digit. The finite error tolerance for the nonlinear system solvers, as well as the accumulation of round-off error, seem to prevent reaching true floating point accuracy.

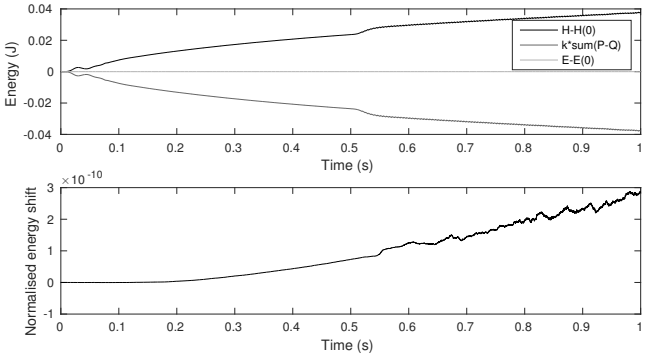

Figure 4: Numerical energy balance for the whole system. Top: in both polarisations, the energy is balanced at all times by the cumulative supplied and withdrawn power. Bottom: the total energy is conserved to the 10th significant digit, when normalised with respect to the mean energy. The apparent trend is due to accumulated round-off error.

5. CONCLUSIONS

This work introduces a novel two polarisation bowed string physical model, including nonlinear damped contact and friction interactions with one bow, one stopping finger, and the distributed fingerboard. An energy-balanced finite difference scheme was presented, resulting in a two-step time recursion. The scheme implementation takes great advantage not only of the structure of Equations 55 and 58, but also of the shape of the nonlinear force term, to optimise computations. In particular, and for this choice of friction curves, the string stopping part of the friction interaction (finger and neck) can, in most realistic playing cases, be decoupled from the highly nonlinear bow part, and solved separately. On the bow side, the use of Friedlander's construction [29] ensures a well-behaved root finding, even trivial during the *sticking* phases of each cycle. Friedlander's

hypothesis, confirmed later experimentally for this type of friction model [23], allows the deterministic resolution of the likely case where the (decoupled) bow part of Equation 58 has not one graphical solution, but three; as a result, a hysteretic cycle arises, leading to pitch flattening. This effect has indeed later been found to be due to the naturally hysteretic thermal behaviour of the melting rosin, indeed well approximated by the simpler friction curve models.

The inclusion of lumped and distributed interactions with the player and fingerboard allows for simulating full articulated gestures in a relatively instinctive and concrete way, without having to rely on somewhat abstract hypotheses — an eloquent example being the finger model, that accounts for several important phenomena that would be difficult (impossible in fact, for some) to model with a simple absorbing string termination. Here, the simple action of pushing a finger down onto the string results in damped dynamic behaviour in both polarisations, variations of the string's speaking length, possible slipping of the string while captured, while the portion of the string between the nut and finger is still realistically oscillating, and responding to the excitation.

However, an important aspect of gestural control in bowed string playing resides in real-time adjustments of playing parameters during note production. The musician relies on immediate feedback from his instrument, adapting its playing accordingly. Our model, even with the aforementioned possible optimisations, does not run in real-time, making gesture design rather difficult. An interesting study could make use of recorded data from sensors during various gestures, feeding them as time series into the model, rather than our current breakpoint functions. This would help calibrate the model, on the string side as well as for the gestural functions [11, 30].

The adaptation of this work to the more realistic case of multiple fingers (and, why not, multiple bows) is trivial, as well as the design of a multiple string environment. The mutual coupling of such strings is the obvious next step, moving towards the design of a full instrument, where strings communicate with a flexible body and with each other through a bridge. The simulated body will eventually take a great part in both the virtual instrument's playability, introducing vibrations feeding back into the strings, and the realism of the synthetic sound; to address the latter, and get a glimpse at the potential of a full instrument model, we have convolved a dry output signal from this string model with the impulse response of a cello body, a principle that is still used to this day for high quality sound synthesis [31]. The resulting sound example can be found online, amongst other relevant samples obtained from the model [1].

6. REFERENCES

[1] L. Hiller and P. Ruiz, "Synthesizing musical sounds by solving the wave equation for vibrating objects: Part 1," *J. Audio Eng. Soc.*, vol. 19, pp. 462–470, June 1971.

[2] R. A. Bacon and J. M. Bowsher, "A discrete model of a struck string," *Acta Acust. united Ac.*, vol. 41, no. 1, pp. 21–27, 1978.

[3] K. Karplus and A. Strong, "Digital synthesis of plucked-string and drum timbres," *Comput. Music J.*, vol. 7, no. 2, pp. 43–55, 1983.

[4] J. O. Smith III, "A new approach to digital reverberation using closed waveguide networks," in *Proc. Int. Computer Music Conf.*, (Vancouver, Canada), pp. 47–53, 1985.

[5] M. Karjalainen, V. Välimäki, and T. Tolonen, "Plucked-string models: from the Karplus-Strong algorithm to digital waveguides and beyond," *Comput. Music J.*, vol. 22, no. 3, pp. 17–32, 1998.

[6] J. Woodhouse, "Physical modeling of bowed strings," *Comput. Music J.*, vol. 16, no. 4, pp. 43–56, 1992.

[7] T. Takala, J. Hiipakka, M. Laurson, and V. Välimäki, "An expressive synthesis model for bowed string instruments," in *Proc. Int. Computer Music Conf.*, (Berlin, Germany), 2000.

[8] S. Serafin, F. Avanzini, D. Ing, and D. Rocchesso, "Bowed string simulation using an elasto-plastic friction model," in *Proc. Stockholm Mus. Acoust. Conf.*, (Stockholm, Sweden), pp. 1–4, 2003.

[9] J. Woodhouse, "Bowed string simulation using a thermal friction model," *Acta Acust. united Ac.*, vol. 89, no. 2, pp. 355–368, 2003.

[10] E. Maestre, C. Spa, and J. O. Smith III, "A bowed string physical model including finite-width thermal friction and hair dynamics," in *Proc. Int. Computer Music Conf.*, (Athens, Greece), 2014.

[11] M. Demoucron, *On the control of virtual violins—Physical modelling and control of bowed string instruments*. PhD thesis, Université Pierre et Marie Curie-Paris VI, 2008.

[12] V. Debut, X. Delaune, and J. Antunes, "Identification of the nonlinear excitation force acting on a bowed string using the dynamical responses at remote locations," *Int. J. Mech. Sci.*, vol. 52, no. 11, pp. 1419–1436, 2010.

[13] J. C. Strikwerda, *Finite difference schemes and partial differential equations*. Siam, 2004.

[14] S. Bilbao, *Numerical sound synthesis*. Chichester, UK: John Wiley & Sons, Ltd, Oct. 2009.

[15] A. Chaigne and A. Askenfelt, "Numerical simulations of piano strings. I. A physical model for a struck string using finite difference methods," *J. Acoust. Soc. Am.*, vol. 95, no. 2, pp. 1112–1118, 1994.

[16] J. Bensa, S. Bilbao, R. Kronland-Martinet, and J. O. Smith III, "The simulation of piano string vibration: From physical models to finite difference schemes and digital waveguides," *J. Acoust. Soc. Am.*, vol. 114, no. 2, pp. 1095–1107, 2003.

[17] S. Bilbao, A. Torin, and V. Chatziioannou, "Numerical modeling of collisions in musical instruments," *Acta Acust. united Ac.*, vol. 101, pp. 155–173, Jan. 2015.

[18] V. Chatziioannou and M. Van Walstijn, "Energy conserving schemes for the simulation of musical instrument contact dynamics," *J. Sound Vib.*, vol. 339, pp. 262–279, 2015.

[19] C. Desvages and S. Bilbao, "Physical modeling of nonlinear player-string interactions in bowed string sound synthesis using finite difference methods," in *Proc. Int. Symp. Mus. Acoust.*, (Le Mans, France), 2014.

[20] S. Bilbao and A. Torin, "Numerical simulation of string/barrier collisions: the fretboard," in *Proc. Int. Conf. Digital Audio Effects*, (Erlangen, Germany), 2014.

[21] M. E. McIntyre and J. Woodhouse, "On the fundamentals of bowed-string dynamics," *Acta Acust. united Ac.*, vol. 43, no. 2, pp. 93–108, 1979.

[22] K. H. Hunt and F. R. E. Crossley, "Coefficient of restitution interpreted as damping in vibroimpact," *J. Appl. Mech.*, vol. 42, no. 2, pp. 440–445, 1975.

[23] J. H. Smith and J. Woodhouse, "The tribology of rosin," *J. Mech. Phys. Solids*, vol. 48, pp. 1633–1681, 2000.

[24] J. Chabassier, *Modeling and numerical simulation of a piano.* Phd thesis, Ecole Polytechnique X, Mar. 2012.

[25] V. Chatziioannou and M. van Walstijn, "An energy conserving finite difference scheme for simulation of collisions," in *Proc. Sound Music Computing Conf.*, (Stockholm, Sweden), pp. 584–591, 2013.

[26] G. K. Percival, *Physical modelling meets machine learning: performing music with a virtual string ensemble*. PhD thesis, University of Glasgow, 2013.

[27] R. T. Schumacher and J. Woodhouse, "The transient behaviour of models of bowed-string motion.," *Chaos (Woodbury, N.Y.)*, vol. 5, no. 3, pp. 509–523, 1995.

[28] J. C. Schelleng, "The bowed string and the player," *J. Acoust. Soc. Am.*, vol. 53, no. 1, pp. 26–41, 1973.

[29] F. G. Friedlander, "On the oscillations of a bowed string," *Math. Proc. Cambridge Phil. Soc.*, vol. 49, pp. 516–530, Oct. 1953.

[30] E. Maestre, "Analysis/synthesis of bowing control applied to violin sound rendering via physical models," in *Proc. Meet. Acoust.*, vol. 19, (Montreal, Canada), p. 035016, 2013.

[31] A. Pérez Carrillo, J. Bonada, J. Patynen, and V. Välimäki, "Method for measuring violin sound radiation based on bowed glissandi and its application to sound synthesis.," *J. Acoust. Soc. Am.*, vol. 130, pp. 1020–9, Aug. 2011.